Two black-hole mergers in public LIGO strain

A two-detector timing and preprocessing study

ABSTRACT

A gravitational-wave chirp recorded by separated detectors may be recognizable in differently conditioned public strain, but the visual resemblance and estimated lag need not be equally stable. We analyzed GW150914 and GW170814 using 32-second Hanford (H1) and Livingston (L1) strain records from the Gravitational Wave Open Science Center. In the primary 35–250 Hz band, cross-correlation in a fixed 250 ms window peaked at H1-minus-L1 lags of +7.36 and +7.75 ms, respectively, with signed correlations of −0.713 and −0.486. All nine combinations of frequency band and noise spectral estimate gave positive lags and negative peaks. The on-source absolute peak exceeded every local synchronous and time-slide control in each setting. For these two excerpts, the ordering of the detector arrivals survived the tested conditioning even as the waveform similarity changed. The resulting timing ranges are sensitivity summaries for known events and the controls are descriptive.

1 Introduction

The discovery paper for GW150914 compared the time-frequency evolution of a short transient in two observatories and showed the overlap of their strain after accounting for relative arrival time and polarity [1]. GW170814 provided a second example of a compact binary merger seen by both LIGO detectors and also by Advanced Virgo [2]. The published parameter estimates use information beyond a local strain correlation. Public, calibrated strain therefore permits a narrower measurement that asks how far a reader can recover a consistent inter-site ordering from the two stretches alone.

Noise color and the inspected frequency range both affect a visual comparison. A narrower band may improve apparent overlap by suppressing unshared noise, while a narrow oscillation band can also produce several competing correlation peaks. A comparison that shows only one aligned superposition leaves these effects implicit. Here we hold the time window and physical search scale fixed across both events and carry the same score to nearby controls. The principal endpoints are the sign and location of the largest absolute correlation. We then measure how much the lag and correlation change across a fixed grid of noise estimates and bands.

GW150914 has the higher network matched-filter signal-to-noise ratio in the discovery reports [1, 2]. We retain H1 and L1 from both events to compare conditioning on a common detector baseline.

2 Data and primary comparison

We used GWTC-1-confident event version 3 for both events [3, 4]. GWOSC lists GPS references of 1126259462.4 and 1186741861.5 s. We read the 4096 Hz HDF5 strain products for H1 and L1, checked matching detector grids, finite samples and continuity of the HDF5 data-present flag over the analysis and control region. Official metadata and file-level hashes are supplied with the code.

3 Conditioning and detectors' peak lag

Let h_i and l_i denote zero-phase-conditioned H1 and L1 on their common native 4096 Hz grid. We evaluated

$$r[k] = \frac{\sum_{i\in W}(h_i - \bar{h})(l_{i-k} - \bar{l}_k)}{\sqrt{\sum_{i\in W}(h_i - \bar{h})^2 \, \sum_{i\in W}(l_{i-k} - \bar{l}_k)^2}}, \qquad W : \ [-160, +90) \text{ ms}.$$

Here $k > 0$ denotes that an H1 feature is later than its L1 counterpart. Each detector mean in the equation is taken on the relevant window. We searched the 83 integer lags from -41 to $+41$ samples, approximately ± 10.01 ms, on the scale of light travel between the observatories. Since the projected strain can have opposite polarity at the two sites, we chose the maximum of $|r[k]|$ and retained the sign and value of $r[k]$ at the winning sample. A three-point parabola on $|r|$ refines the location of an interior maximum. The absolute score reported below remains the observed maximum on the native grid.

Noise spectrum and filtering. For each site we estimated a noise power spectrum from the two intervals $[-14, -8)$ and $[8, 14)$ s relative to the catalog time. The primary estimate pooled Hann-windowed one-second periodograms with 50% overlap and took their median by frequency. We used spectra rather than concatenating strain at the training-interval junction. After a three-bin median smoother, we interpolated the log spectrum onto the FFT grid, multiplied the Fourier coefficients by inverse square root power, and transformed back to time. The full record was mean centered and Tukey tapered ($\alpha = 0.125$) with four seconds of zero padding on each side before the FFT. We applied a forward–reverse fourth-order Butterworth bandpass using second-order sections and then removed the padding. The fit evaluates strains deep inside the tapered record. Doubling the padding in the primary pipeline changed the peak lag by at most 0.000007 ms and signed correlation by less than 2×10^{-6} for these two excerpts.

Control design. We repeated the same lag search on 46 synchronous off-source windows with shifts at integer multiples of 0.25 s from -6.75 to -1.25 s and from $+1.25$ to $+6.75$ s. For each of the 23 negative and 23 positive offsets, we paired H1 and L1 windows across opposite signs in both orders, making 1,058 pairs. Each of the resulting scores uses the same width, the same lag search and the same preprocessing as the event. The local reference tests how the on-source score compares with nearby strain under matched conditions.

Sensitivity and validation. We crossed three passbands (30–180, 35–250 and 45–350 Hz) with three spectral estimators (median 1 s, mean 1 s and median 2 s). There were nine settings per event, including the primary analysis. A separate noiseless synthetic chirp with known fractional shifts verified the lag sign and parabolic refinement. A monotonic test curve verified endpoint flagging. The native sample interval is approximately 0.244 ms. Interpolation of the correlation peak is numerical and does not calibrate statistical timing error.

Figure transformations. Figure 1 uses frequency-localized Gaussian energy for the morphological views. For each frequency, the Gaussian envelope has standard deviation $5/(2\pi f)$, and the energy for each detector is divided by its own off-source median before averaging in linear units. These maps use native sample times. Waveform panels show whitened and filtered strain in units of each detector's local noise RMS. For display only, L1 is linearly interpolated at the refined alignment lag and sign-inverted. The correlation score is calculated before that display transform.

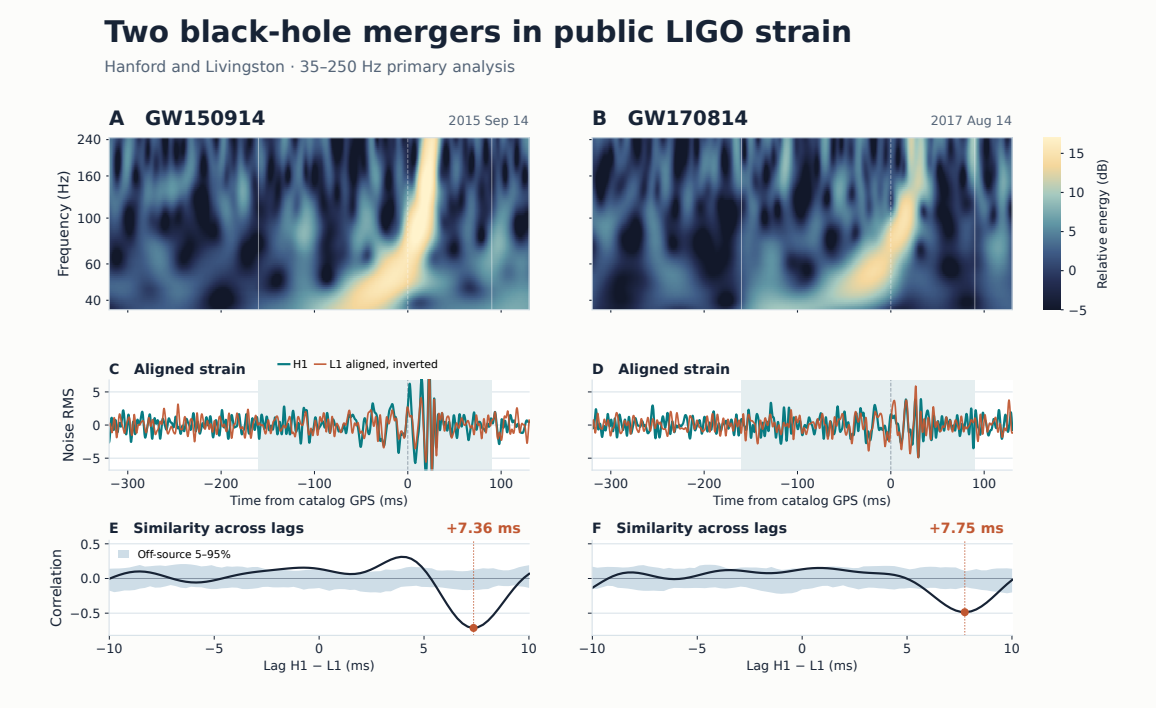


Figure 1: **Morphology and lag in the primary 35–250 Hz analysis.** (A,B) Time–frequency energy averaged across detectors on the native time grid relative to their local off-source median energy. Vertical rules mark the 250 ms analysis window and catalog GPS reference (dashed). (C,D) Conditioned H1 and aligned, sign-inverted L1 in local noise RMS. Shading identifies the window used to compute the correlations. (E,F) Signed Pearson correlation at each trial lag. The shaded band gives the pointwise 5th to 95th percentiles of the 46 synchronous off-source correlation curves. Red marks show the peak selected by absolute correlation. Off-source shading describes local samples and provides no significance estimate. Positive lag means H1 receives the corresponding feature later than L1.

4 Results

Arrival order is consistent across settings. Both on-source strain records show an increase in concentrated time–frequency energy near the catalog reference (Fig. 1A,B). After applying the primary lag and polarity, the short oscillatory structure in the event window is shared across sites (Fig. 1C,D). The extremum on the signed correlation curve is negative in each case (Fig. 1E,F). GW150914 has the larger absolute primary peak, 0.713 compared with 0.486 for GW170814. The two lags are consistent with Livingston leading Hanford by about 7 ms in the first discovery paper [1] and about 8 ms in the second [2].

Local control scores fall below the on-source peaks. In the primary setting no synchronous or time-slide control reached the on-source score for either event. The same ordering held when the band and spectral estimator were varied. Figure 2 shows the timing alongside the time-slide distribution summaries for each choice. The H1-minus-L1 lag ranged from 7.28 to 7.54 ms for GW150914 (span 0.27 ms from unrounded estimates) and 7.65 to 8.00 ms for GW170814 (span 0.35 ms). The signed peak remained negative in all settings. The largest primary synchronous and time-slide magnitudes were 0.295 and 0.453 for GW150914 and 0.301 and 0.404 for GW170814. The 1,058 time-slide pairs reuse 46 available offsets per detector.

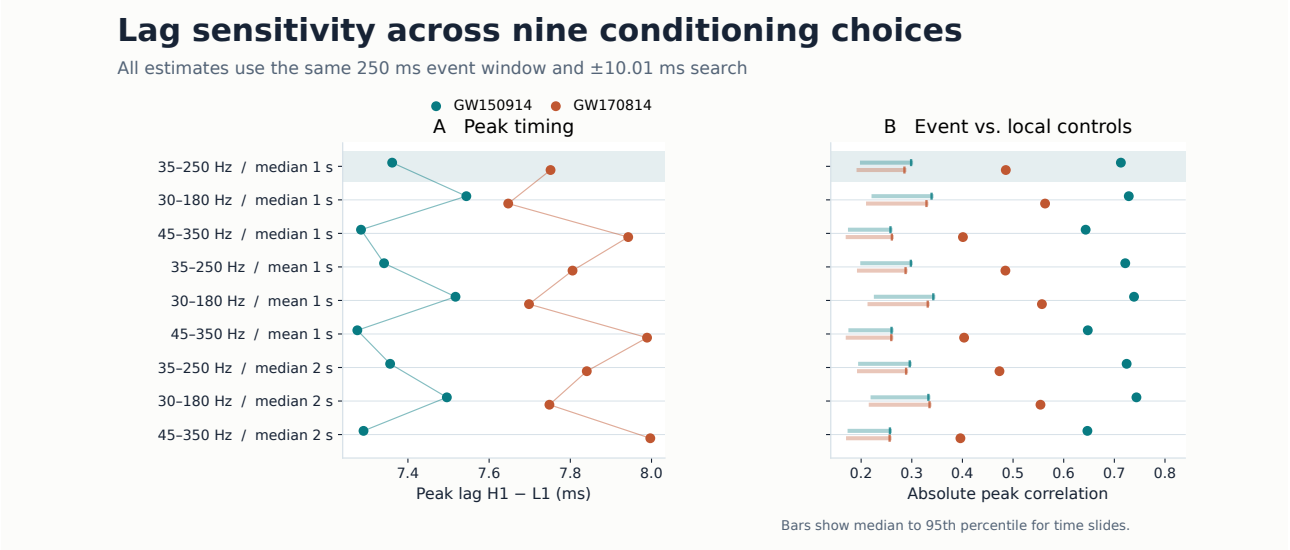


Figure 2: **Settings reveal different sensitivity in timing and correlation.** (A) Peaks after crossing three passbands and three noise-spectrum settings. The shaded row is the primary analysis. (B) Filled points show the measured on-source peak magnitude. Short horizontal bars extend from the median to the 95th percentile of the corresponding time-slide control scores. These are descriptive percentiles. Spectral labels give estimator and Hann segment length.

5 Discussion

A single score would hide the distinction between aligning the two detectors in time and making their waveforms look more similar. For example, limiting the passband to 30–180 Hz increased peak similarity relative to the primary band in both excerpts. Expanding the high end to 350 Hz while removing frequencies below 45 Hz reduced it. This common direction is consistent with an effect of changing the mixture of visible chirp and detector noise, but these three overlapping bands vary both cutoffs and do not isolate which Fourier components are responsible.

The control windows compare nearby portions of the same released products. They share the estimated noise spectra and time-slide pairs repeatedly use the same 46 offsets per detector. Zero exceedances among these dependent pairs conveys local separation. Estimating a false-alarm probability or rate would require a search calibration across substantially more observing time with an explicit accounting of the selection and background. We also lack a statistical uncertainty on the delays. The bands and PSDs sample analysis choices, and the associated spread reflects conditioning among those choices. A network timing inference would instead need a model for signal, calibration and noise. For GW170814, that analysis would also retain Virgo measurements to exploit the network geometry [2].

The workflow provides a reproducible way to examine aligned fluctuations in public strain while checking how dependent a visual impression is on conditioning. These results connect the published ordering of arrivals to an explicit fixed-window measurement and distinguish that ordering from the observed amplitude of the correlation peak.

Data, software and scope

The GWOSC versioned event metadata and original HDF5 file links used in this work are bundled as a provenance table and official catalog JSON. The public release is archived under 10.7935/82H3-HH23. This work was a secondary analysis of released calibrated strain. The bundle includes the protocol, complete per-setting peak and control summaries, plotting inputs derived from those records, analysis and plotting scripts, an editable LaTeX manuscript and SVG figure files. The four source strain records are retrieved independently from GWOSC. The artifacts include the exact file SHA-256 values for reruns.

Acknowledgments. This research has made use of data or software obtained from the Gravitational Wave Open Science Center (gwosc.org), a service of the LIGO Scientific Collaboration, the Virgo Collaboration, and KAGRA. LIGO is funded by the U.S. National Science Foundation. Virgo is funded by the French Centre National de Recherche Scientifique (CNRS), the Italian Istituto Nazionale della Fisica Nucleare (INFN) and the Dutch Nikhef, with contributions by Polish and Hungarian institutes.

References

[1] B. P. Abbott et al. (LIGO Scientific Collaboration and Virgo Collaboration). Observation of gravitational waves from a binary black hole merger. *Phys. Rev. Lett.* **116**, 061102 (2016). 10.1103/PhysRevLett.116.061102.

[2] B. P. Abbott et al. (LIGO Scientific Collaboration and Virgo Collaboration). GW170814: A three-detector observation of gravitational waves from a binary black hole coalescence. *Phys. Rev. Lett.* **119**, 141101 (2017). 10.1103/PhysRevLett.119.141101.

[3] Gravitational Wave Open Science Center. GWTC-1 confident-event catalog and strain release. Version 3 records for GW150914 and GW170814. 10.7935/82H3-HH23.

[4] R. Abbott et al. (LIGO Scientific Collaboration and Virgo Collaboration). Open data from the first and second observing runs of Advanced LIGO and Advanced Virgo. *SoftwareX* **13**, 100658 (2021). 10.1016/j.softx.2021.100658.